ABAQUS implementation of strain gradient plasticity

E. Martínez-Pañeda[a,*]

[a]*Department of Engineering, University of Cambridge*

Abstract

Documentation that accompanies the file UELSGP.f - a user element subroutine (UEL) with an implicit implementation of modern strain gradient plasticity (see Gudmundson, 2004; Fleck and Willis, 2009) incorporating both dissipative and energetic higher order contributions. If using this code for research or industrial purposes, please cite:

E. Martínez-Pañeda, V.S. Deshpande, C.F. Niordson, N.A. Fleck. The role of plastic strain gradients in the crack growth resistance of metals. Journal of the Mechanics and Physics of Solids 126: 136-150 (2019)

Keywords:
Strain gradient plasticity, Finite element analysis, Higher-order, ABAQUS, Backward Euler

1. Introduction

In recent years there has been an increasing interest in characterizing the behaviour of metallic materials at the micrometer scale. Examples are found in micro-electromechanical systems (MEMS), microelectronic components and thin film applications. A wide array of micron scale experiments have revealed that metals display strong size effects when deformed non uniformly into the plastic range. Particularly representative examples are: (i) indentation [1], (ii) torsion [2] and (iii) bending [3]. Size effects are not observed under uniaxial tension and therefore the *smaller is harder* or *smaller is stronger* trends observed in the aforementioned experiments are intrinsically associated with the presence of strain gradients. At the continuum

*Corresponding author.
Email address: mail@empaneda.com (E. Martínez-Pañeda)

scale, Strain Gradient Plasticity (SGP) theories have been proposed to extend conventional plasticity theory to small scales. Grounded on the physical notion of Geometrically Necessary Dislocations (GNDs), associated with incompatibility due to strain gradients, SGP theories relate the plastic work (or, in some cases, the yield strength) to both strains and strain gradients; thereby introducing a length scale in the material description. These models are cast in a form which reduces to classic plasticity when the length scales of the imposed deformation gradients are large compared to the material length parameters.

Size effects have an important influence in a number of fields beyond micron-scale applications as plastic strains vary over microns in a wide range of engineering designs. Among other, SGP have proven to be fundamental in modelling fracture [4, 5], fatigue [6, 7], strengthening on TRIP steels and fiber-reinforced materials [8, 9], hydrogen embrittlement [10, 11], friction and contact [12, 13], void growth [14], and damage [15, 16]. However, a comprehensive embrace of SGP models has been long hindered by the complexities associated with their numerical implementation. This is particularly true in structural integrity assessment and other large scale applications that demand a robust and efficient computational framework requiring, at the same time, a very fine characterization to capture the micron-scale phenomena governing the macroscopic response [17]. We here provide a robust implicit implementation of advanced gradient plasticity theories in the well-known finite element package ABAQUS.

2. Strain Gradient Plasticity

We adopt Gudmundson's SGP model [18], as it is probably the most popular gradient plasticity formulation proposed so far, and incorporates both the influence of energetic and dissipative contributions. The code can be easily modified to model size effects by means of other strain gradient plasticity formulations.

2.1. Principle of virtual work and governing equations

Employing a small strain formulation, the total strain rate is determined from the gradients of the displacement rates: $\dot{\varepsilon}_{ij} = \left(\dot{u}_{i,j} + \dot{u}_{j,i}\right)/2$, and decomposes into an elastic part, $\dot{\varepsilon}^e_{ij}$, and a plastic part, $\dot{\varepsilon}^p_{ij}$, so that: $\dot{\varepsilon}_{ij} = \dot{\varepsilon}^e_{ij} + \dot{\varepsilon}^p_{ij}$.

For a solid of volume V and external surface S, the principle of virtual work reads,

$$\int_V \left(\sigma_{ij}\delta\varepsilon^e_{ij} + q_{ij}\delta\varepsilon^p_{ij} + \tau_{ijk}\delta\varepsilon^p_{ij,k}\right)dV = \int_S \left(T_i\delta u_i + t_{ij}\delta\varepsilon^p_{ij}\right)dS \qquad (1)$$

where σ_{ij} denotes the Cauchy stress, q_{ij} the so-called micro-stress tensor (work conjugate to the plastic strain, ε^p_{ij}) and τ_{ijk} the higher order stress tensor (work conjugate to the plastic strain gradients $\varepsilon^p_{ij,k}$), being the prime symbol omitted from q_{ij} and τ_{ijk} although only their deviatoric parts contribute to the principle of virtual work. The right-hand side of Eq. (1) includes both conventional tractions, $T_i = \sigma_{ij}n_j$, and higher order terms, $t_{ij} = \tau_{ijk}n_k$, with n_k denoting the outward normal to the surface S. The principle of virtual work can alternatively be stated as

$$\int_V \left(\sigma_{ij}\delta\varepsilon_{ij} + \left(q_{ij} - \sigma'_{ij}\right)\delta\varepsilon^p_{ij} + \tau_{ijk}\delta\varepsilon^p_{ij,k}\right)dV = \int_S \left(T_i\delta u_i + t_{ij}\delta\varepsilon^p_{ij}\right)dS \qquad (2)$$

Here, σ'_{ij} is the deviatoric part of the Cauchy stress: $\sigma'_{ij} = \sigma_{ij} - \delta_{ij}\sigma_{kk}/3$. Applying the product rule and Gauss' divergence theorem to the internal virtual work - left hand side of Eq. (2) - renders

$$\begin{aligned}\delta W_i = \int_S \left(\sigma_{ij}n_j\delta u_i + \tau_{ijk}n_k\delta\varepsilon^p_{ij}\right)dS - \int_V \Big(&\sigma_{ij,j}\delta u_i \\ &+ \left(\tau_{ijk,k} + s_{ij} - q_{ij}\right)\delta\varepsilon^p_{ij}\Big)dV\end{aligned} \qquad (3)$$

Since the second integral on the right-hand side of Eq. (3) should vanish for arbitrary variations, two sets of equilibrium equations can be obtained

$$\sigma_{ij,j} = 0 \qquad (4)$$

$$\tau_{ijk,k} + s_{ij} - q_{ij} = 0 \qquad (5)$$

Where the first integral on the right hand side of (3) may be identified as part of the external virtual work. Thus, by accounting for the right hand side of (1), the corresponding conventional $T_i = \sigma_{ij}n_j$ and higher order $t_{ij} = \tau_{ijk}n_k$ boundary conditions can be obtained.

2.2. Constitutive prescriptions

Dissipative higher order contributions can be incorporated - in a thermodynamically consistent manner - by employing higher order stress quantities

that are related to increments of strain, as postulated by Gudmundson [18] and Gurtin and Anand [19]. The pivotal step in constructing this class of constitutive relations is to define an effective stress Σ work conjugate to the gradient-enhanced effective plastic strain rate $\dot{E}^p$, ensuring that the plastic work rate,

$$\Sigma \dot{E}^p = q_{ij}\dot{\varepsilon}^p_{ij} + \tau^D_{ijk}\dot{\varepsilon}^p_{ij,k} \tag{6}$$

is always positive. Such that, for a quadratic form of the gradient enhanced effective plastic strain rate,

$$\dot{E}^p = \sqrt{\frac{2}{3}\dot{\varepsilon}^p_{ij}\dot{\varepsilon}^p_{ij} + L^2\dot{\varepsilon}^p_{ij,k}\dot{\varepsilon}^p_{ij,k}} \tag{7}$$

where L is the dissipative length scale; a work conjugate effective stress can be defined

$$\Sigma = \sqrt{\frac{2}{3}q^D_{ij}q^D_{ij} + L^{-2}\tau^D_{ijk}\tau^D_{ijk}} \tag{8}$$

and the corresponding dissipative stress quantities (in terms of *increments* of strain) can be readily obtained:

$$q^D_{ij} = \frac{2}{3}\frac{\Sigma}{\dot{E}^p}\dot{\varepsilon}^p_{ij} \quad \text{and} \quad \tau^D_{ijk} = \frac{\Sigma}{\dot{E}^p}L^2\dot{\varepsilon}^p_{ij,k} \tag{9}$$

Following [18], the energetic contributions are obtained from the free energy, with a quadratic form being assumed,

$$\Psi = \frac{1}{2}\left(\varepsilon_{ij} - \varepsilon^p_{ij}\right)C_{ijkl}\left(\varepsilon_{kl} - \varepsilon^p_{kl}\right) + \frac{1}{2}\mu\ell^2\varepsilon^p_{ij,k}\varepsilon^p_{ij,k} \tag{10}$$

Here, C_{ijkl} is the isotropic elastic stiffness tensor, μ the shear modulus and ℓ the energetic constitutive length parameter. The conventional stresses are given through the elastic relationship:

$$\sigma_{ij} = \frac{\partial\Psi}{\partial\varepsilon^e_{ij}} = C_{ijkl}\left(\varepsilon_{kl} - \varepsilon^p_{kl}\right) \tag{11}$$

And the energetic higher order stresses are derived as:

$$\tau^E_{ijk} = \frac{\partial\Psi}{\partial\varepsilon^p_{ij,k}} = \mu\ell^2\varepsilon^p_{ij,k} \tag{12}$$

3. Numerical implementation

Quantitative assessment of gradient effects in engineering applications has been long hindered by the difficulties in the numerical implementation of higher order strain gradient plasticity theories. The vast majority of the numerical frameworks proposed consider only dissipative or energetic terms, but not both. A notable exception are the works by Niordson and co-workers [20–22], where a Forward Euler time integration scheme is employed. Very recently, Panteghini and Bardella [23] implemented Gurtin (2004) model [24] in an implicit scheme by using a special viscoplastic potential. Here, for the first time, Gudmundson [18] formulation is implemented within a Backward Euler framework, including both dissipative and energetic contributions. This is largely facilitated by the definition of a new viscoplastic potential able to model both rate dependent and rate independent behavior by extending the work of Panteghini and Bardella [23].

3.1. Viscoplastic law

Gradient plasticity theories are generally implemented within a rate-dependent setting, taking advantage of its well-known computational capabilities and circumventing complications in the corresponding time independent model associated with identifying active plastic zones [20, 21]. In the context of rate-dependent gradient plasticity models, an effective flow resistance Σ is defined,

$$\Sigma\left(\dot{E}^p, E^p\right) = \sigma_F\left(E^p\right) V\left(\dot{E}^p\right) \tag{13}$$

which is work conjugated to the gradient-enhanced effective plastic flow rate $\dot{E}^p$. Here, σ_F is the current flow stress, which depends on the initial yield stress σ_Y and the hardening law. Several viscoplastic laws have been proposed in the literature; a common one (as in, e.g., [22]) is the following,

$$\mathscr{V}\left(\dot{E}^p, E^p\right) = \frac{\sigma_F\left(E^p\right)\dot{\varepsilon}_0}{m+1}\left(\frac{\dot{E}^p}{\dot{\varepsilon}_0}\right)^{m+1} \tag{14}$$

so that

$$\Sigma\left(\dot{E}^p, E^p\right) = \sigma_F V(\dot{E}^p) = \sigma_F\left(E^p\right)\left(\frac{\dot{E}^p}{\dot{\varepsilon}_0}\right)^{m} \tag{15}$$

with m being the rate sensitivity exponent, $\dot{\varepsilon}_0$ the reference strain rate and $V(\dot{E}^p)$ the viscoplastic function.

Two numerical problems arise; first, the initial tangent is infinite; and second, the derivative of Σ (i.e., $\partial\Sigma/\partial\dot{E}^p$) tends to infinity if $\dot{E}^p \to 0$, with the effect that the system to solve in the finite element algorithm is ill-conditioned for small $\dot{E}^p$. To overcome the first problem, Martínez-Pañeda et al. [22] adopt the following visco-plastic function,

$$V(\dot{E}^p) = \begin{cases} \frac{\dot{E}^p}{\dot{\varepsilon}_0}\varpi^{(1-1/m)} & \text{if } \frac{\dot{E}^p}{\dot{\varepsilon}_0} \leq \varpi^{1/m} \\ \left(\frac{\dot{E}^p}{\dot{\varepsilon}_0}\right)^m & \text{if } \frac{\dot{E}^p}{\dot{\varepsilon}_0} > \varpi^{1/m} \end{cases} \tag{16}$$

Here, ϖ is a numerical parameter that has to be sufficiently small (< 0.4, approx.). This implies a rough linearization of the first part of the $V(\dot{E}^p)$ vs $\dot{E}^p$ curve. On the other hand, Panteghini and Bardella [23] suggest to deal with the two issues mentioned before by means of the following viscoplastic function,

$$V(\dot{E}^p) = \begin{cases} \frac{\dot{E}^p}{2\dot{\varepsilon}_0} & \text{if } \frac{\dot{E}^p}{\dot{\varepsilon}_0} \leq 1 \\ 1 - \frac{\dot{\varepsilon}_0}{2\dot{E}^p} & \text{if } \frac{\dot{E}^p}{\dot{\varepsilon}_0} > 1 \end{cases} \tag{17}$$

This approach is computationally very robust, as $\partial\Sigma/\partial\dot{E}^p$ (for the simple case where $\sigma_F(E^p) = \sigma_Y$) equals,

$$\frac{\partial\Sigma}{\partial\dot{E}^p} = \begin{cases} \sigma_Y \frac{1}{2\dot{\varepsilon}_0} & \text{if } \frac{\dot{E}^p}{\dot{\varepsilon}_0} \leq 1 \\ \sigma_Y \frac{\dot{\varepsilon}_0}{2(\dot{E}^p)^2} & \text{if } \frac{\dot{E}^p}{\dot{\varepsilon}_0} > 1 \end{cases} \tag{18}$$

such that, when $\dot{E} \to 0$ the contribution of $\partial\Sigma/\partial\dot{E}^p$ will remain bounded. The sole limitation of this viscoplastic function is that it does not allow to model rate-dependent behaviour (i.e., it is very appropriate to attain the rate independent limit but not so much to study the influence of m). Fuentes-Alonso and Martínez-Pañeda [25] proposed the following law,

$$V(\dot{E}^p) = \begin{cases} \frac{\dot{E}^p}{\varpi\dot{\varepsilon}_0} & \text{if } \frac{\dot{E}^p m}{\dot{E}^p_*} \leq 1 \\ \left(\frac{\dot{E}^p - \frac{1-m}{m}\dot{E}^p_*}{\dot{\varepsilon}_0}\right)^m & \text{if } \frac{\dot{E}^p m}{\dot{E}^p_*} > 1 \end{cases} \tag{19}$$

with ϖ being a regularization parameter that takes values around 0.01 (larger values improve convergence, smaller values approximate in a more accurate way the power law). A smooth transition is obtained by computing the critical $\dot{E}^p_*$ from the relation between the derivatives,

$$\dot{E}^p_* = \dot{\varepsilon}_0 \left(\frac{1}{\varpi m}\right)^{1/(m-1)} \tag{20}$$

and by offsetting the curve a distance ϕ. This distance corresponds to the intersection between the abscissa axis and the tangent line at the critical point. From the relation,

$$V'_* = \frac{V_*}{\phi + \dot{E}^p_*} \Rightarrow \phi = \frac{V_*}{V'_*} - \dot{E}^p_* \tag{21}$$

one can easily compute V_*/V'_*,

$$\frac{V_*}{V'_*} = \frac{(\dot{E}^p)^m/\dot{\varepsilon}_0^m}{\frac{m}{\dot{\varepsilon}_0}\left(\frac{\dot{E}^p}{\dot{\varepsilon}_0}\right)^{m-1}} = \frac{\dot{E}^p}{m} \tag{22}$$

And going back to (21), we can now solve,

$$\phi = \frac{\dot{E}^p_*}{m} - \dot{E}^p_* = \frac{1-m}{m}\dot{E}^p_* \tag{23}$$

In that way we are able to reproduce a mechanical response that follows accurately the classic viscoplastic power law while providing with a robust numerical framework. The shape of the curves is shown in Fig. 1 for the particular case of $m = 0.05$, $\dot{\varepsilon}_0 = 1$ s^{-1} (in the case of [23] an equivalent $\dot{\varepsilon}_0 = 10^3$ s^{-1} is employed).

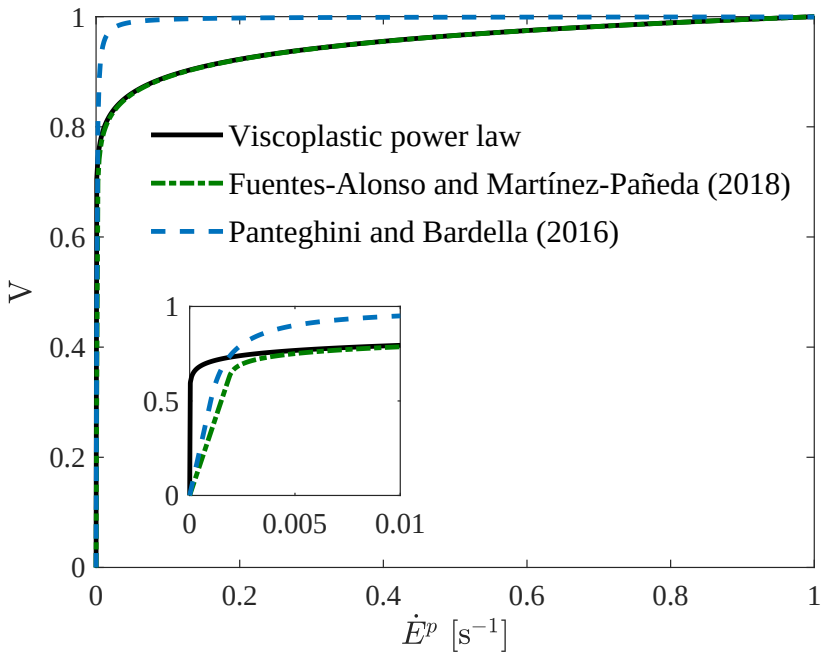

Figure 1: Comparison between the classic viscoplastic power law, the viscoplastic function by Fuentes-Alonso and Martínez-Pañeda [25] and the proposal by Panteghini and Bardella [23]. In the latter the reference strain rate $\dot{\varepsilon}_0$ equals 10^3 s^{-1}, while in the other two cases a rate sensitivity exponent of $m = 0.05$ and a reference strain rate $\dot{\varepsilon}_0 = 1$ are adopted.

The derivative of the viscoplastic function must be computed to build stiffness matrix. For the present proposal, within the simplest case of $\sigma_F = \sigma_Y$, equals,

$$\frac{\partial \Sigma}{\partial \dot{E}^p} = \begin{cases} \frac{\sigma_Y}{\varpi \dot{\varepsilon}_0} & \text{if } \frac{\dot{E}^p m}{\dot{E}^p_*} \leq 1 \\ \sigma_Y \frac{m}{\dot{\varepsilon}_0} \left(\frac{\dot{E}^p - \frac{1-m}{m} \dot{E}^p_*}{\varepsilon_0} \right)^{m-1} & \text{if } \frac{\dot{E}^p m}{\dot{E}^p_*} > 1 \end{cases} \tag{24}$$

The three approaches outlined (Martínez-Pañeda et al. [22], Panteghini and Bardella [23], and Fuentes-Alonso and Martínez-Pañeda [25]) have been implemented in the user element subroutine with the choice being made through a flag variable in the input file.

3.2. Finite element implementation

A robust and fully implicit (Backward Euler) implementation of strain gradient plasticity is carried out in the popular finite element package ABAQUS.

The formulation described in Section 2 is implemented by means of a user element subroutine. Plane strain conditions are assumed for simplicity (the extension to three dimensions is nevertheless straightforward) and quadrilateral elements with 5 degrees of freedom per node are employed. For the sake of clarity Voigt notation is used and matrices are denoted by double underline. Such that the increment of the vectorial field variable $\underline{a}$ within the time step is given by,

$$\Delta \underline{a} = \dot{\underline{a}} \Delta t \tag{25}$$

We therefore solve at the nodes for the following primal variables: $\Delta \hat{u}_x$, $\Delta \hat{u}_y$, $\Delta \hat{\varepsilon}^p_{xx}$, $\Delta \hat{\varepsilon}^p_{yy}$ and $\Delta \hat{\gamma}^p_{xy}$. And for a given value of such variables, its value at the Gauss integration point is first obtained,

$$\Delta \underline{\varepsilon}\left(\xi, \eta\right) = \underline{\underline{B}}\left(\xi, \eta\right) \Delta \underline{\hat{u}} \tag{26}$$

$$\Delta \underline{\varepsilon}^p\left(\xi, \eta\right) = \underline{\underline{N_{\varepsilon^p}}}\left(\xi, \eta\right) \Delta \underline{\hat{\varepsilon}}^p \tag{27}$$

$$\Delta \underline{\nabla \varepsilon}^p\left(\xi, \eta\right) = \underline{\underline{M_{\nabla \varepsilon^p}}}\left(\xi, \eta\right) \Delta \underline{\hat{\varepsilon}}^p \tag{28}$$

$$\underline{\nabla \varepsilon}^p\left(\xi, \eta\right) = \underline{\underline{M_{\nabla \varepsilon^p}}}\left(\xi, \eta\right) \underline{\hat{\varepsilon}}^p \tag{29}$$

where, for a number of nodes $\hat{n}$,

$$\underline{\hat{u}} = \begin{bmatrix} \hat{u}_x^{(1)} & \hat{u}_y^{(1)} & \cdots & \hat{u}_x^{(\hat{n})} & \hat{u}_y^{(\hat{n})} \end{bmatrix}^T \tag{30}$$

$$\underline{\hat{\varepsilon}}^p = \begin{bmatrix} \hat{\varepsilon}_x^{p\,(1)} & \hat{\varepsilon}_y^{p\,(1)} & \hat{\gamma}_{xy}^{p\,(1)} & \cdots & \hat{\varepsilon}_x^{p\,(\hat{n})} & \hat{\varepsilon}_y^{p\,(\hat{n})} & \hat{\gamma}_{xy}^{p\,(\hat{n})} \end{bmatrix}^T \tag{31}$$

$$\underline{\underline{B}} = \begin{bmatrix} \frac{\partial N^{(1)}}{\partial x} & 0 & \cdots & \frac{\partial N^{(\hat{n})}}{\partial x} & 0 \\ 0 & \frac{\partial N^{(1)}}{\partial y} & \cdots & 0 & \frac{\partial N^{(\hat{n})}}{\partial y} \\ 0 & 0 & \cdots & 0 & 0 \\ \frac{\partial N^{(1)}}{\partial y} & \frac{\partial N^{(1)}}{\partial x} & \cdots & \frac{\partial N^{(\hat{n})}}{\partial y} & \frac{\partial N^{(\hat{n})}}{\partial x} \end{bmatrix} \tag{32}$$

$$\underline{\underline{N_{\varepsilon^p}}} = \begin{bmatrix} N^{(1)} & 0 & 0 & \cdots & N^{(\hat{n})} & 0 & 0 \\ 0 & N^{(1)} & 0 & \cdots & 0 & N^{(\hat{n})} & 0 \\ -N^{(1)} & -N^{(1)} & 0 & \cdots & -N^{(\hat{n})} & -N^{(\hat{n})} & 0 \\ 0 & 0 & N^{(1)} & \cdots & 0 & 0 & N^{(\hat{n})} \end{bmatrix} \tag{33}$$

$$\underline{\underline{M_{\nabla\varepsilon^p}}} = \begin{bmatrix} \frac{\partial N^{(1)}}{\partial x} & 0 & 0 & \cdots & \frac{\partial N^{(\hat{n})}}{\partial x} & 0 & 0 \\ \frac{\partial N^{(1)}}{\partial y} & 0 & 0 & \cdots & \frac{\partial N^{(\hat{n})}}{\partial y} & 0 & 0 \\ 0 & \frac{\partial N^{(1)}}{\partial x} & 0 & \cdots & 0 & \frac{\partial N^{(\hat{n})}}{\partial x} & 0 \\ 0 & \frac{\partial N^{(1)}}{\partial y} & 0 & \cdots & 0 & \frac{\partial N^{(\hat{n})}}{\partial y} & 0 \\ -\frac{\partial N^{(1)}}{\partial x} & -\frac{\partial N^{(1)}}{\partial x} & 0 & \cdots & -\frac{\partial N^{(\hat{n})}}{\partial x} & -\frac{\partial N^{(\hat{n})}}{\partial x} & 0 \\ -\frac{\partial N^{(1)}}{\partial y} & -\frac{\partial N^{(1)}}{\partial y} & 0 & \cdots & -\frac{\partial N^{(\hat{n})}}{\partial y} & -\frac{\partial N^{(\hat{n})}}{\partial y} & 0 \\ 0 & 0 & \frac{\partial N^{(1)}}{\partial x} & \cdots & 0 & 0 & \frac{\partial N^{(\hat{n})}}{\partial x} \\ 0 & 0 & \frac{\partial N^{(1)}}{\partial y} & \cdots & 0 & 0 & \frac{\partial N^{(\hat{n})}}{\partial y} \end{bmatrix} \tag{34}$$

The 4x4 elastic stiffness matrix $\underline{\underline{L}}$ is then built from the values of E and ν, and the stress updated,

$$\underline{\sigma} = \underline{\sigma}_n + \underline{\underline{L}}\left(\Delta\underline{\varepsilon} - \Delta\underline{\varepsilon}^p\right) \tag{35}$$

The generalized gradient-enhanced effective plastic strain increment is then computed according to,

$$\Delta E^p = \sqrt{\frac{2}{3}\Delta\underline{\varepsilon}^{p^T}\underline{\underline{H_\varepsilon}}\Delta\underline{\varepsilon}^p + L^2\Delta\underline{\nabla\varepsilon}^{p^T}\underline{\underline{H_{\nabla\varepsilon}}}\Delta\underline{\nabla\varepsilon}^p} \tag{36}$$

where $\underline{\underline{H_\varepsilon}}$ and $\underline{\underline{H_{\nabla\varepsilon}}}$ are diagonal matrices which link the Voigt and tensorial notations,

$$\underline{\underline{H_\varepsilon}} = \begin{bmatrix} 1 & 0 & 0 & 0 \\ 0 & 1 & 0 & 0 \\ 0 & 0 & 1 & 0 \\ 0 & 0 & 0 & 1/2 \end{bmatrix} \tag{37}$$

$$\underline{\underline{H_{\nabla\varepsilon}}} = \begin{bmatrix} 1 & 0 & 0 & 0 & 0 & 0 & 0 & 0 \\ 0 & 1 & 0 & 0 & 0 & 0 & 0 & 0 \\ 0 & 0 & 1 & 0 & 0 & 0 & 0 & 0 \\ 0 & 0 & 0 & 1 & 0 & 0 & 0 & 0 \\ 0 & 0 & 0 & 0 & 1 & 0 & 0 & 0 \\ 0 & 0 & 0 & 0 & 0 & 1 & 0 & 0 \\ 0 & 0 & 0 & 0 & 0 & 0 & 1/2 & 0 \\ 0 & 0 & 0 & 0 & 0 & 0 & 0 & 1/2 \end{bmatrix} \tag{38}$$

We then compute the flow stress,

$$\sigma_F\left(E^p + \Delta E^p\right) = \sigma_Y\left(1 + \frac{E\left(E^p + \Delta E^p\right)}{\sigma_Y}\right)^N \tag{39}$$

and its derivative with respect to ΔE^p, as it will be needed to compute $\partial\Sigma/\partial\Delta E^p$,

$$\frac{\partial\sigma_F\left(E^p+\Delta E^p\right)}{\partial\Delta E^p}=NE\left(1+\frac{E\left(E^p+\Delta E^p\right)}{\sigma_Y}\right)^{N-1} \tag{40}$$

The effective flow resistance, $\Sigma=\sigma_F(E^p)V\left(\Delta E^p/\Delta t\right)$, is then computed according to the viscoplastic law. We then proceed to update the unconventional dissipative stresses,

$$\underline{q}^D=\frac{2}{3}\frac{\Sigma}{\Delta E^p}\underline{\underline{H_\varepsilon}}\Delta\underline{\varepsilon}^p \tag{41}$$

$$\underline{\tau}^D=L^2\frac{\Sigma}{\Delta E^p}\underline{\underline{H_{\nabla\varepsilon}}}\Delta\underline{\nabla\varepsilon}^p \tag{42}$$

We update E^p and the most relevant strain quantities (for visualization purposes),

$$\underline{\varepsilon}^p=\underline{\varepsilon}^p_n+\Delta\underline{\varepsilon}^p \tag{43}$$

$$\underline{\varepsilon}=\underline{\varepsilon}_n+\Delta\underline{\varepsilon} \tag{44}$$

$$E^p=E^p+\Delta E^p \tag{45}$$

We compute the energetic higher order stresses,

$$\underline{\tau}^E=\mu\ell^2\underline{\underline{H_{\nabla\varepsilon}}}\underline{\nabla\varepsilon}^p \tag{46}$$

and finally we compute the right hand side (residual) and the element stiffness matrix. Note that the discretized form of the internal virtual work is given by,

$$W_i=\int_\Omega\left\{\underline{\sigma}^T\underline{\underline{B}}\delta\underline{\hat{u}}+\left[(\underline{q}^D-\underline{\sigma})^T\underline{\underline{N_{\varepsilon^p}}}+\underline{\tau}^T\underline{\underline{M_{\nabla\varepsilon^p}}}\right]\delta\underline{\hat{\varepsilon}}^p\right\}dV \tag{47}$$

Differentiating this last expression with respect to the variation of the nodal variables $\delta\underline{\hat{u}}$ and $\delta\underline{\hat{\varepsilon}}^p$ leads to the vectors at the right-hand-sides of the following equations,

$$\underline{R}_u=\int_\Omega\underline{\underline{B}}^T\underline{\sigma}dV \tag{48}$$

$$\underline{R}_{\varepsilon^p}=\int_\Omega\left[\underline{\underline{N_{\varepsilon^p}}}^T(\underline{q}^D-\underline{\sigma})+\underline{\underline{M_{\nabla\varepsilon^p}}}^T\underline{\tau}\right]dV \tag{49}$$

The *consistent* stiffness matrix $\underline{\underline{K}}$, required to complete the FE algorithm and assure second-order convergence of the NewtonRaphson scheme

employed is defined as the differentiation of the residuals with respect to the incremental nodal variables. The element stiffness matrix is constructed with the following distribution per each nodal block,

$$\underline{\underline{K}} = \begin{bmatrix} \underline{\underline{K}}_{u,u} & \underline{\underline{K}}_{u,\varepsilon^p} \\ \underline{\underline{K}}_{\varepsilon^p,u} & \underline{\underline{K}}_{\varepsilon^p,\varepsilon^p} \end{bmatrix} \tag{50}$$

with,

$$\underline{\underline{K}}_{u,u} = \int_\Omega \underline{\underline{B}}^T \underline{\underline{L}}\, \underline{\underline{B}} dV \tag{51}$$

$$\underline{\underline{K}}_{u,\varepsilon^p} = -\int_\Omega \underline{\underline{B}}^T \underline{\underline{L}}\, \underline{\underline{N_{\varepsilon^p}}} dV \tag{52}$$

$$\underline{\underline{K}}_{\varepsilon^p,u} = -\int_\Omega \underline{\underline{N_{\varepsilon^p}}}^T \underline{\underline{L}}\, \underline{\underline{B}} dV \tag{53}$$

$$\begin{aligned} \underline{\underline{K}}_{\varepsilon^p,\varepsilon^p} = \int_\Omega \Bigg\{ & \underline{\underline{N_{\varepsilon^p}}}^T \left[\left(\frac{\partial \underline{q}^D}{\partial \Delta \underline{\varepsilon}^p} + \underline{\underline{L}} \right) \underline{\underline{N_{\varepsilon^p}}} + \frac{\partial \underline{q}^D}{\partial \Delta \underline{\nabla \varepsilon}^p} \underline{\underline{M_{\nabla \varepsilon^p}}} \right] \\ & + \underline{\underline{M_{\nabla \varepsilon^p}}}^T \left(\frac{\partial \underline{\tau}^D}{\partial \Delta \underline{\varepsilon}^p} \underline{\underline{N_{\varepsilon^p}}} + \frac{\partial \underline{\tau}^D}{\partial \Delta \underline{\nabla \varepsilon}^p} \underline{\underline{M_{\nabla \varepsilon^p}}} + \frac{\partial \underline{\tau}^E}{\partial \underline{\nabla \varepsilon}^p} \underline{\underline{M_{\nabla \varepsilon^p}}} \right) \Bigg\} dV \end{aligned} \tag{54}$$

and,

$$\frac{\partial \Delta E^p}{\partial \Delta \underline{\varepsilon}^p} = \frac{2}{3\Delta E^p} \left(\underline{\underline{H_\varepsilon}} \Delta \underline{\varepsilon}^p \right)^T \tag{55}$$

$$\frac{\partial \Delta E^p}{\partial \Delta \underline{\nabla \varepsilon}^p} = \frac{L^2}{\Delta E^p} \left(\underline{\underline{H_{\nabla \varepsilon}}} \Delta \underline{\nabla \varepsilon}^p \right)^T \tag{56}$$

$$\frac{\partial \underline{q}^D}{\partial \Delta \underline{\varepsilon}^p} = \frac{2}{3} \underline{\underline{H_\varepsilon}} \Delta \underline{\varepsilon}^p \left(\frac{1}{\Delta E^p} \frac{\partial \Sigma}{\partial \Delta E^p} - \frac{\Sigma}{(\Delta E^p)^2} \right) \frac{\partial \Delta E^p}{\partial \Delta \underline{\varepsilon}^p} + \frac{2}{3} \underline{\underline{H_\varepsilon}} \frac{\Sigma}{\Delta E^p} \tag{57}$$

$$\frac{\partial \underline{q}^D}{\partial \Delta \underline{\nabla \varepsilon}^p} = \frac{2}{3} \underline{\underline{H_\varepsilon}} \Delta \underline{\varepsilon}^p \left(\frac{1}{\Delta E^p} \frac{\partial \Sigma}{\partial \Delta E^p} - \frac{\Sigma}{(\Delta E^p)^2} \right) \frac{\partial \Delta E^p}{\partial \Delta \underline{\nabla \varepsilon}^p} \tag{58}$$

$$\frac{\partial \underline{\tau}^D}{\partial \Delta \underline{\varepsilon}^p} = L^2 \underline{\underline{H_{\nabla \varepsilon}}} \Delta \underline{\nabla \varepsilon}^p \left(\frac{1}{\Delta E^p} \frac{\partial \Sigma}{\partial \Delta E^p} - \frac{\Sigma}{(\Delta E^p)^2} \right) \frac{\partial \Delta E^p}{\partial \Delta \underline{\varepsilon}^p} \tag{59}$$

$$\frac{\partial \underline{\tau}^D}{\partial \Delta \underline{\nabla \varepsilon}^p} = L^2 \underline{\underline{H_{\nabla \varepsilon}}} \Delta \underline{\nabla \varepsilon}^p \left(\frac{1}{\Delta E^p} \frac{\partial \Sigma}{\partial \Delta E^p} - \frac{\Sigma}{(\Delta E^p)^2} \right) \frac{\partial \Delta E^p}{\partial \Delta \underline{\nabla \varepsilon}^p} + L^2 \underline{\underline{H_{\nabla \varepsilon}}} \frac{\Sigma}{\Delta E^p} \tag{60}$$

Comprehensive details of the derivation are given in Appendix A.

4. Usage instructions

A very simple example is provided to ease the use of the subroutine. As in [20], we will analyse size effects in an homogeneous finite slab clamped between rigid platens and subjected to tensile loading. A square slab is considered ($h = w$) and all the components of the displacement field are constrained at $x_2 = h$ and $x_2 = 0$ (see Fig. 2). A vertical displacement rate of $\dot{\Delta} = h\dot{\varepsilon}_0/10$ is imposed in the upper edge ($x_2 = h$). As in [20], the following material properties are adopted: $\sigma_Y/E = 0.001$, $\nu = 0.3$, $N = 0.1$, and $\dot{\varepsilon}_0 = 0.001$. A uniform mesh of 400 quadrilateral quadratic plane strain finite elements is employed.

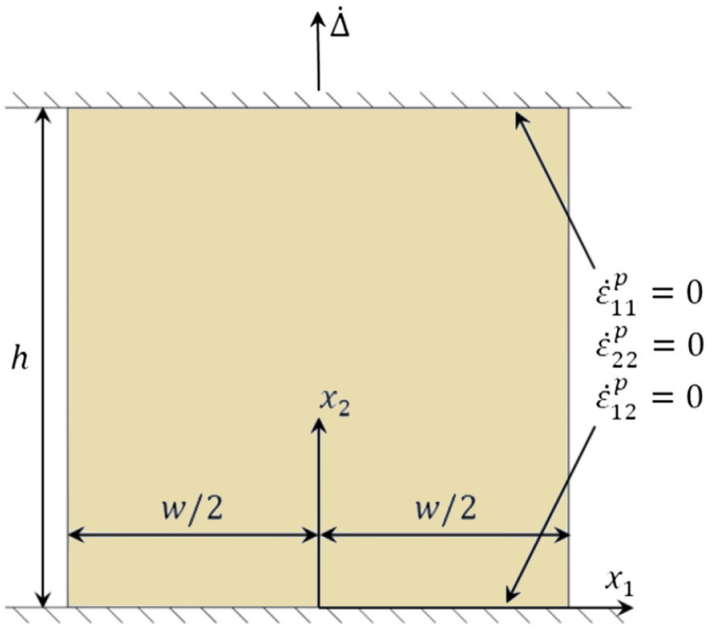

Figure 2: Geometry and boundary conditions for a finite slab of homogeneous material constrained between rigid platens.

First, we create the model in Abaqus/CAE following the usual procedure and meshing with CPE8 elements. The input file is then edited (by, e.g., using Notepad++) to accommodate the file for the user element (UEL) subroutine. The first change involves the definition of the user element, one should replace:

```
*Element, type=CPE8
```

by,

```
*USER ELEMENT,TYPE=U1,NODES=8,COORDINATES=2,PROPERTIES=9,VAR=117
1,2,3,4,5
*ELEMENT, TYPE=U1, ELSET=SOLID
```

where we specify the number of nodes, coordinates, properties and state variables, along with the degrees of freedom (from 1 to 5: $\Delta\hat{u}_x$, $\Delta\hat{u}_y$, $\Delta\hat{\varepsilon}^p_{xx}$, $\Delta\hat{\varepsilon}^p_{yy}$, $\Delta\hat{\gamma}^p_{xy}$). After the element connectivity listing we introduce the 10 element properties outlined before,

```
*UEL PROPERTY, ELSET=SOLID
1.,0.3,0.001,0.25,0.01,0.03,0.1,0.05,
1
```

in this way the variables of the analysis can be defined without modifying the Fortran code. The 9 user-defined properties employed in the UEL subroutine are described in Table 1.

Table 1: Equivalence between the properties and the corresponding variables.

PROPS	Variable
1	E - Young's modulus
2	ν - Poisson's ratio
3	σ_Y - Initial yield stress
4	ℓ - Energetic length scale parameter
5	L - Dissipative length scale parameter
6	$\dot{\varepsilon}_0$ - Reference strain rate
7	N - Strain hardening exponent
8	m - Rate sensitivity exponent
9	Viscoplastic flag variable (1 - [25], 2- [22], 3 - [23])

For this problem we choose to assign a Young's modulus of 1 and an initial yield stress of 0.001 to keep the ratio $\sigma_Y/E = 0.001$ (as in [20]). Poisson's ratio equals $\nu = 0.3$ and the strain hardening exponent $N = 0.1$. We choose to reproduce the curve for $\ell = h/4$ and $L = h/100$. Since we created a squared model of dimensions 1x1 (i.e., $h = 1$) we define $\ell = 0.25$ and $L = 0.01$. To reproduce the results by Nielsen and Niordson [20] showing the influence of

the strain rate sensitivity, we use the viscoplastic potential recently proposed by Fuentes-Alonso and Martínez-Pañeda (i.e., flag variable equal to 1). In [20] they load at a fixed rate $\dot{\Delta} = h\dot{\varepsilon}_0/10$ with $\dot{\varepsilon}_0 = 0.001$ (i.e., $\dot{\Delta} = 0.0001$) and the prescribed displacement goes up to $\Delta/(h\varepsilon_Y) = 3$. Since $h = 1$ and $\varepsilon_Y = \sigma_Y/E = 0.001$ then $\Delta = 0.003$, implying a total loading step time of 30 s for $\dot{\Delta} = 0.0001$. We will stick to Abaqus' default option of a total step time of 1 s and, therefore, in our case the equivalent scenario is: $\dot{\Delta} = 0.003$ and $\dot{\varepsilon}_0 = 0.03$ ($\dot{\varepsilon}_0$ scales linearly with the time step).

Optionally, we can define a "phantom mesh" so as to visualize results in Abaqus/Viewer as this is not possible when using user elements. By writing a very simple user material (UMAT) subroutine we can define elements with a stiffness matrix equal to zero, avoiding any influence on the simulation, and at the same time store the results as solution dependent variables that we can request as output. We include with the files a Matlab script (VirtualMesh.m), which is part of the Abaqus2Matlab package [26], that reads the original (unmodified) input file created in Abaqus/CAE (named `Job-1.inp`) and automatically creates a new file (`Job-1a.inp`) with the listing of the dummy mesh by increasing the number of elements by one order of magnitude. We copy and paste this information in the input file and add a name for the set of elements:

```
*Element, type=cpe8, elset=output
1001,    1,    2,   23,   22,  442,  443,  444,  445
1002,    2,    3,   24,   23,  446,  447,  448,  44
...
```

Then we edit the definition of our solid section to refer to this set,

```
*Solid Section, elset=output, material=user
```

Accordingly we define our material as a user material, so as to transfer the output from the UEL subroutine to the UMAT subroutine and visualize it in Abaqus/Viewer.

```
*Material, name=user
*Depvar
     29
1, S11, S11
2, S22, S22
```

```
3, S33, S33
4, S12, S12
5, E11, E11
6, E22, E22
7, E33, E33
8, E12, E12
9, EP11, EP11
10, EP22, EP22
11, EP33, EP33
12, EP12, EP12
13, Td111, Td111
14, Td112, Td112
15, Td221, Td221
16, Td222, Td222
17, Td331, Td331
18, Td332, Td332
19, Td121, Td121
20, Td122, Td122
21, Te111, Te111
22, Te112, Te112
23, Te221, Te221
24, Te222, Te222
25, Te331, Te331
26, Te332, Te332
27, Te121, Te121
28, Te122, Te122
29, EP, EP
*User Material, constants=1
400.,
```

The only user property defined in the material is the number of elements of the model (400). Optionally, we assign names to the user dependent variables to ease the interpretation of the results in the code (in this way, the equivalence of each state variable is self-explanatory).

Finally, when using higher order SGP models we may want to take advantage of one of their strengths: the capability of prescribing boundary conditions on the plastic strains. In this boundary value problem we choose

to equate to zero all ε_{ij}^{p} components at the top and the bottom of the plate. We do that by adding boundary conditions related to the degrees of freedom 3, 4 and 5:

```
** Name: Bottom Type: Displacement/Rotation
*Boundary
Set-1, 1, 1
Set-1, 2, 2
Set-1, 3, 3
Set-1, 4, 4
Set-1, 5, 5
```

and,

```
** Name: Top Type: Displacement/Rotation
*Boundary
Set-2, 2, 2, 0.003
Set-1, 3, 3
Set-1, 4, 4
Set-1, 5, 5
```

Additionally, one should remember to request the variable `SDV` in the field output request to visualize results,

```
*Element Output, directions=YES
SDV,
```

The results obtained by means of the present numerical implementation, along with those reported in [20], are shown in Fig. 3. A Python script is provided to ease the computation of the results. Different values of the length scale parameters and the rate sensitivity exponent have been considered. A very good agreement with the numerical results by Nielsen and Niordson [20] is observed in all cases. The code is very robust and, even for a case of $m = 0.001$ - that mimics the rate-independent result of [20] - the problem is solved with a total of 10 iterations. The implementation has been further validated by comparing with the simple shear results of Niordson and Legarth [27] and the bending results of Idiart et al. [28].

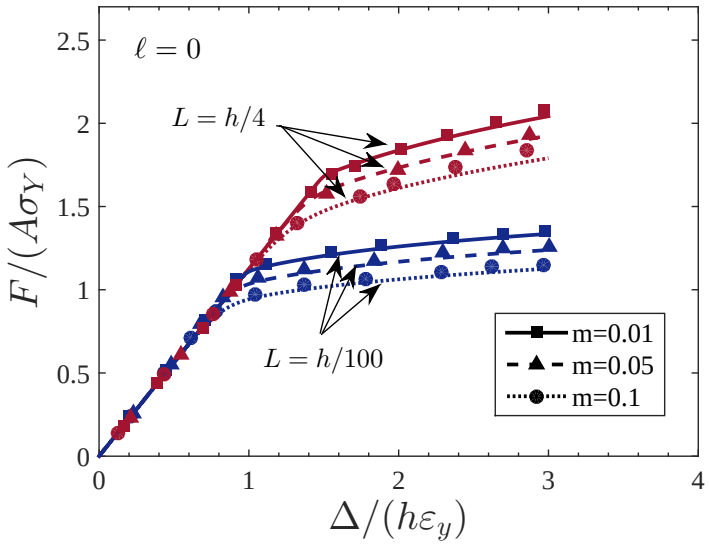

(a)

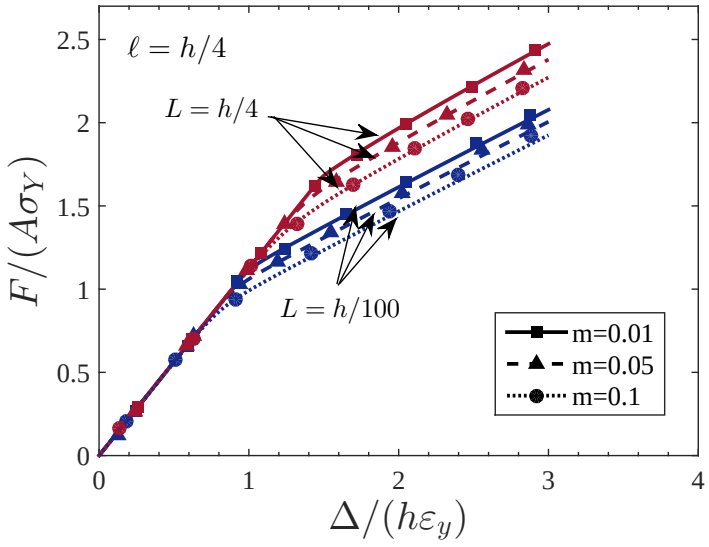

(b)

Figure 3: Material response curves for a clamped slab subjected to tensile loading. Numerical results from the present numerical implementation (lines) and Nielsen and Niordson [20] (symbols) for (a) $\ell = 0$ and (b) $\ell = h/4$ and different values of L and the rate sensitivity exponent m. Other parameters: $A = wt$ and $\varepsilon_y = \sigma_Y/E$.

5. Conclusions

If the code and the documentation provided here are useful please cite:

E. Martínez-Pañeda, V.S. Deshpande, C.F. Niordson, N.A. Fleck. The role of plastic strain gradients in the crack growth resistance of metals. Journal of the Mechanics and Physics of Solids 126: 136-150 (2019)

Do not hesitate to contact for further clarifications. Further details can be found in the Supplementary Material of the main paper [29].

6. Acknowledgments

E. Martínez-Pañeda acknowledges financial support from the People Programme (Marie Curie Actions) of the European Union's Seventh Framework Programme (FP7/2007-2013) under REA grant agreement n° 609405 (COFUNDPostdocDTU).

Appendix A. Derivation of the stiffness matrix

$$\frac{\partial \Delta E^p}{\partial \Delta \underline{\varepsilon}^p} = \frac{1}{2\sqrt{\frac{2}{3}\Delta \underline{\varepsilon}^{p^T} \underline{\underline{H_\varepsilon}} \Delta \underline{\varepsilon}^p + L^2 \Delta \underline{\nabla \varepsilon}^{p^T} \underline{\underline{H_{\nabla\varepsilon}}} \Delta \underline{\nabla \varepsilon}^p}} \frac{4}{3} \left(\underline{\underline{H_\varepsilon}} \Delta \underline{\varepsilon}^p \right)^T$$
$$= \frac{2}{3\Delta E^p} \left(\underline{\underline{H_\varepsilon}} \Delta \underline{\varepsilon}^p \right)^T \tag{A.1}$$

$$\frac{\partial \Delta E^p}{\partial \Delta \underline{\nabla \varepsilon}^p} = \frac{1}{2\sqrt{\frac{2}{3}\Delta \underline{\varepsilon}^{p^T} \underline{\underline{H_\varepsilon}} \Delta \underline{\varepsilon}^p + L^2 \Delta \underline{\nabla \varepsilon}^{p^T} \underline{\underline{H_{\nabla\varepsilon}}} \Delta \underline{\nabla \varepsilon}^p}} 2L^2 \left(\underline{\underline{H_{\nabla\varepsilon}}} \Delta \underline{\nabla \varepsilon}^p \right)^T$$
$$= \frac{L^2}{\Delta E^p} \left(\underline{\underline{H_{\nabla\varepsilon}}} \Delta \underline{\nabla \varepsilon}^p \right)^T \tag{A.2}$$

$$\begin{aligned}
\frac{\partial \underline{q}^D}{\partial \Delta \underline{\varepsilon}^p} &= \frac{2}{3}\underline{\underline{H_\varepsilon}}\left(\frac{\Sigma}{\Delta E^p} + \Delta\underline{\varepsilon}^p \frac{\partial\left(\Sigma/\Delta E^p\right)}{\partial \Delta \underline{\varepsilon}^p}\right) \\
&= \frac{2}{3}\underline{\underline{H_\varepsilon}}\left[\frac{\Sigma}{\Delta E^p} + \Delta\underline{\varepsilon}^p\left(\Sigma\frac{\partial\left(1/\Delta E^p\right)}{\partial \Delta \underline{\varepsilon}^p} + \frac{1}{\Delta E^p}\frac{\partial \Sigma}{\partial \Delta \underline{\varepsilon}^p}\right)\right] \\
&= \frac{2}{3}\underline{\underline{H_\varepsilon}}\left[\frac{\Sigma}{\Delta E^p} + \Delta\underline{\varepsilon}^p\left(\Sigma\frac{\partial\left(1/\Delta E^p\right)}{\partial \Delta E^p}\frac{\partial \Delta E^p}{\partial \Delta \underline{\varepsilon}^p} + \frac{1}{\Delta E^p}\frac{\partial \Sigma}{\partial \Delta E^p}\frac{\partial \Delta E^p}{\partial \Delta \underline{\varepsilon}^p}\right)\right] \\
&= \frac{2}{3}\underline{\underline{H_\varepsilon}}\left[\frac{\Sigma}{\Delta E^p} + \Delta\underline{\varepsilon}^p\frac{\partial \Delta E^p}{\partial \Delta \underline{\varepsilon}^p}\left(-\frac{\Sigma}{\left(\Delta E^p\right)^2} + \frac{1}{\Delta E^p}\frac{\partial \Sigma}{\partial \Delta E^p}\right)\right] \qquad \text{(A.3)}
\end{aligned}$$

$$\begin{aligned}
\frac{\partial \underline{q}^D}{\partial \Delta \underline{\nabla \varepsilon}^p} &= \frac{2}{3}\underline{\underline{H_\varepsilon}}\Delta\underline{\varepsilon}^p\frac{\partial\left(\Sigma/\Delta E^p\right)}{\partial \Delta \underline{\nabla \varepsilon}^p} = \frac{2}{3}\underline{\underline{H_\varepsilon}}\Delta\underline{\varepsilon}^p\left(\Sigma\frac{\partial\left(1/\Delta E^p\right)}{\partial \Delta \underline{\nabla \varepsilon}^p} + \frac{1}{\Delta E^p}\frac{\partial \Sigma}{\partial \Delta \underline{\nabla \varepsilon}^p}\right) \\
&= \frac{2}{3}\underline{\underline{H_\varepsilon}}\Delta\underline{\varepsilon}^p\left(\Sigma\frac{\partial\left(1/\Delta E^p\right)}{\partial \Delta E^p}\frac{\partial \Delta E^p}{\partial \Delta \underline{\nabla \varepsilon}^p} + \frac{1}{\Delta E^p}\frac{\partial \Sigma}{\partial \Delta E^p}\frac{\partial \Delta E^p}{\partial \Delta \underline{\nabla \varepsilon}^p}\right) \\
&= \frac{2}{3}\underline{\underline{H_\varepsilon}}\Delta\underline{\varepsilon}^p\frac{\partial \Delta E^p}{\partial \Delta \underline{\nabla \varepsilon}^p}\left(-\frac{\Sigma}{\left(\Delta E^p\right)^2} + \frac{1}{\Delta E^p}\frac{\partial \Sigma}{\partial \Delta E^p}\right) \qquad \text{(A.4)}
\end{aligned}$$

$$\begin{aligned}
\frac{\partial \underline{T}^D}{\partial \Delta \underline{\varepsilon}^p} &= L^2\underline{\underline{H_{\nabla\varepsilon}}}\Delta\underline{\nabla\varepsilon}^p\frac{\partial\left(\Sigma/\Delta E^p\right)}{\partial \Delta \underline{\varepsilon}^p} = L^2\underline{\underline{H_{\nabla\varepsilon}}}\Delta\underline{\nabla\varepsilon}^p\left(\Sigma\frac{\partial\left(1/\Delta E^p\right)}{\partial \Delta \underline{\varepsilon}^p} + \frac{1}{\Delta E^p}\frac{\partial \Sigma}{\partial \Delta \underline{\varepsilon}^p}\right) \\
&= L^2\underline{\underline{H_{\nabla\varepsilon}}}\Delta\underline{\nabla\varepsilon}^p\left(\Sigma\frac{\partial\left(1/\Delta E^p\right)}{\partial \Delta \underline{\varepsilon}^p} + \frac{1}{\Delta E^p}\frac{\partial \Sigma}{\partial \Delta \underline{\varepsilon}^p}\right) \\
&= L^2\underline{\underline{H_{\nabla\varepsilon}}}\Delta\underline{\nabla\varepsilon}^p\left(\Sigma\frac{\partial\left(1/\Delta E^p\right)}{\partial \Delta E^p}\frac{\partial \Delta E^p}{\partial \Delta \underline{\varepsilon}^p} + \frac{1}{\Delta E^p}\frac{\partial \Sigma}{\partial \Delta E^p}\frac{\partial \Delta E^p}{\partial \Delta \underline{\varepsilon}^p}\right) \\
&= L^2\underline{\underline{H_{\nabla\varepsilon}}}\Delta\underline{\nabla\varepsilon}^p\frac{\partial \Delta E^p}{\partial \Delta \underline{\varepsilon}^p}\left(-\frac{\Sigma}{\left(\Delta E^p\right)^2} + \frac{1}{\Delta E^p}\frac{\partial \Sigma}{\partial \Delta E^p}\right) \qquad \text{(A.5)}
\end{aligned}$$

$$
\begin{aligned}
\frac{\partial \underline{T}^D}{\partial \Delta \underline{\nabla \varepsilon}^p} &= L^2 \underline{\underline{\underline{\underline{H_{\nabla\varepsilon}}}}} \left(\frac{\Sigma}{\Delta E^p} + \Delta \underline{\nabla \varepsilon}^p \frac{\partial \left(\Sigma / \Delta E^p \right)}{\partial \Delta \underline{\nabla \varepsilon}^p} \right) \\
&= L^2 \underline{\underline{\underline{\underline{H_{\nabla\varepsilon}}}}} \left[\frac{\Sigma}{\Delta E^p} + \Delta \underline{\nabla \varepsilon}^p \left(\Sigma \frac{\partial \left(1/\Delta E^p \right)}{\partial \Delta \underline{\nabla \varepsilon}^p} + \frac{1}{\Delta E^p} \frac{\partial \Sigma}{\partial \Delta \underline{\nabla \varepsilon}^p} \right) \right] \\
&= L^2 \underline{\underline{\underline{\underline{H_{\nabla\varepsilon}}}}} \left[\frac{\Sigma}{\Delta E^p} + \Delta \underline{\nabla \varepsilon}^p \left(\Sigma \frac{\partial \left(1/\Delta E^p \right)}{\partial \Delta E^p} \frac{\partial \Delta E^p}{\partial \Delta \underline{\nabla \varepsilon}^p} + \frac{1}{\Delta E^p} \frac{\partial \Sigma}{\partial \Delta E^p} \frac{\partial \Delta E^p}{\partial \Delta \underline{\nabla \varepsilon}^p} \right) \right] \\
&= L^2 \underline{\underline{\underline{\underline{H_{\nabla\varepsilon}}}}} \left[\frac{\Sigma}{\Delta E^p} + \Delta \underline{\nabla \varepsilon}^p \frac{\partial \Delta E^p}{\partial \Delta \underline{\nabla \varepsilon}^p} \left(- \frac{\Sigma}{\left(\Delta E^p \right)^2} + \frac{1}{\Delta E^p} \frac{\partial \Sigma}{\partial \Delta E^p} \right) \right]
\end{aligned}
\tag{A.6}
$$

References

[1] W. D. Nix, H. J. Gao, Indentation size effects in crystalline materials: A law for strain gradient plasticity, Journal of the Mechanics and Physics of Solids 46 (3) (1998) 411–425. doi:10.1016/s0022-5096(97)00086-0.

[2] N. A. Fleck, G. M. Muller, M. F. Ashby, J. W. Hutchinson, Strain gradient plasticity: Theory and Experiment, Acta Metallurgica et Materialia 42 (2) (1994) 475–487.

[3] J. S. Stölken, A. G. Evans, A microbend test method for measuring the plasticity length scale, Acta Materialia 46 (14) (1998) 5109–5115.

[4] E. Martínez-Pañeda, C. Betegón, Modeling damage and fracture within strain-gradient plasticity, International Journal of Solids and Structures 59 (2015) 208–215.

[5] E. Martínez-Pañeda, C. F. Niordson, On fracture in finite strain gradient plasticity, International Journal of Plasticity 80 (2016) 154–167.

[6] S. Brinckmann, T. Siegmund, Computations of fatigue crack growth with strain gradient plasticity and an irreversible cohesive zone model, Engineering Fracture Mechanics 75 (8) (2008) 2276–2294.

[7] S. Brinckmann, T. Siegmund, A cohesive zone model based on the micromechanics of dislocations, Modelling and Simulation in Materials Science & Engineering 16 (2008) 065003 (19pp).

[8] L. Mazzoni-Leduc, T. Pardoen, T. J. Massart, Strain gradient plasticity analysis of transformation induced plasticity in multiphase steels, International Journal of Solids and Structures 45 (20) (2008) 5397–5418.

[9] B. N. Legarth, C. F. Niordson, Debonding failure and size effects in micro-reinforced composites, International Journal of Plasticity 26 (1) (2010) 149–165.

[10] E. Martínez-Pañeda, S. del Busto, C. F. Niordson, C. Betegón, Strain gradient plasticity modeling of hydrogen diffusion to the crack tip, International Journal of Hydrogen Energy 41 (24) (2016) 10265–10274.

[11] E. Martínez-Pañeda, C. F. Niordson, R. P. Gangloff, Strain gradient plasticity-based modeling of hydrogen environment assisted cracking, Acta Materialia 117 (2016) 321–332.

[12] H. Song, E. Van der Giessen, X. Liu, Strain gradient plasticity analysis of elasto-plastic contact between rough surfaces, Journal of the Mechanics and Physics of Solids 96 (2016) 18–28.

[13] K. L. Nielsen, C. F. Niordson, J. W. Hutchinson, Rolling at small scales, Journal of Manufacturing Science and Engineering, Transactions of the ASME 138 (4) (2016) 1–10.

[14] C. F. Niordson, V. Tvergaard, Size-effects in porous metals, Modelling and Simulation in Materials Science and Engineering 15.

[15] R. K. Abu Al-Rub, G. Z. Voyiadjis, A finite strain plastic-damage model for high velocity impact using combined viscosity and gradient localization limiters: Part I - Theoretical formulation, Vol. 15, 2006.

[16] E. C. Aifantis, Internal length gradient (ILG) material mechanics across scales and disciplines, Advances in Applied Mechanics 49 (2016) 1–110.

[17] E. Martínez-Pañeda, S. Natarajan, S. Bordas, Gradient plasticity crack tip characterization by means of the extended finite element method, Computational Mechanics 59 (2017) 831–842.

[18] P. Gudmundson, A unified treatment of strain gradient plasticity, Journal of the Mechanics and Physics of Solids 52 (6) (2004) 1379–1406.

[19] M. E. Gurtin, L. Anand, A theory of strain-gradient plasticity for isotropic, plastically irrotational materials. Part I: Small deformations, International Journal of the Mechanics and Physics of Solids 53 (2005) 1624–1649.

[20] K. L. Nielsen, C. F. Niordson, A 2D finite element implementation of the Fleck-Willis strain-gradient flow theory, European Journal of Mechanics, A/Solids 41 (2013) 134–142.

[21] K. L. Nielsen, C. F. Niordson, A numerical basis for strain-gradient plasticity theory: Rate-independent and rate-dependent formulations, Journal of the Mechanics and Physics of Solids 63 (1) (2014) 113–127.

[22] E. Martínez-Pañeda, C. F. Niordson, L. Bardella, A finite element framework for distortion gradient plasticity with applications to bending of thin foils, International Journal of Solids and Structures 96 (2016) 288–299.

[23] A. Panteghini, L. Bardella, On the Finite Element implementation of higher-order gradient plasticity, with focus on theories based on plastic distortion incompatibility, Computer Methods in Applied Mechanics and Engineering 310 (2016) 840–865.

[24] M. E. Gurtin, A gradient theory of small-deformation isotropic plasticity that accounts for the Burgers vector and for dissipation due to plastic spin, Journal of the Mechanics and Physics of Solids 52 (11) (2004) 2545–2568.

[25] S. Fuentes-Alonso, E. Martínez-Pañeda, Fracture in distortion gradient plasticity, (submitted).

[26] G. Papazafeiropoulos, M. Muñiz-Calvente, E. Martínez-Pañeda, Abaqus2Matlab: A suitable tool for finite element post-processing, Advances in Engineering Software 105 (2017) 9–16.

[27] C. F. Niordson, B. N. Legarth, Strain gradient effects on cyclic plasticity, Journal of the Mechanics and Physics of Solids 58 (4) (2010) 542–557.

[28] M. I. Idiart, V. S. Deshpande, N. A. Fleck, J. R. Willis, Size effects in the bending of thin foils, International Journal of Engineering Science 47 (11-12) (2009) 1251–1264.

[29] E. Martínez-Pañeda, V. S. Deshpande, C. F. Niordson, N. A. Fleck, The role of plastic strain gradients in the crack growth resistance of metals, Journal of the Mechanics and Physics of Solids 126 (2019) 136–150.